Importance of the band gap energy and flat band potential for application of modified TiO$_2$ photoanodes in water photolysis

M. Radecka [a,*], M. Rekas [a], A. Trenczek-Zajac [a], K. Zakrzewska [b]

[a] *Faculty of Material Science and Ceramics, AGH-University of Science and Technology, al. Mickiewicza 30, 30-059 Krakow, Poland*
[b] *Faculty of Electrical Engineering, Automatics, Computer Science and Electronics, AGH-University of Science and Technology, al. Mickiewicza 30, 30-059 Krakow, Poland*

Abstract

The influence on water photolysis of two important parameters of the electronic structure of photocatalytic semiconductors: the forbidden band gap, E_g, that decides about the absorption spectrum and the flat band potential, V_{Fb}, that affects the recombination probability, was studied. The photoelectrochemical experiments were performed in a three-electrode cell PEC with a TiO$_2$ thin film photoanode immersed in liquid electrolyte of variable pH. Titanium dioxide photoanodes doped with chromium (up to 16 at.%) and tin (up to 50 at.%) were prepared by rf reactive sputtering. Different methods of flat band potential determination: Mott–Schottky plots and photocurrent versus voltage characteristics were used. The energy band gap was derived from the spectrophotometric measurements of optical transmittance and reflectance coefficients of thin films. For TiO$_2$ + 7.6 at.% Cr high and negative flat band potential $V_{Fb} = -0.72$ eV (at pH 4) has been found but the recombination time $\tau = 8$ s was the shortest of all TiO$_2$ modifications. Despite additional absorption feature at about 2.8 eV, i.e., at wavelength corresponding to visible range of the light spectrum, the photoconversion efficiency of TiO$_2$ + 7.6 at.% Cr was found to be much smaller ($\eta_c = 0.1\%$) than that of undoped TiO$_2$ ($\eta_c = 1.8\%$) and TiO$_2$ doped with 8 at.% of Sn ($\eta_c = 1.0\%$).
© 2007 Elsevier B.V. All rights reserved.

Keywords: Titanium dioxide; Flat band potential; Forbidden band gap; Photoelectrochemical cell; Water photolysis; Hydrogen generation

1. Introduction

Photoelectrochemical splitting of water is an environmentally friendly method of hydrogen generation based on renewable and apparently unlimited natural resources such as water and solar energy. Assisted by solar radiation, direct splitting of water into molecular hydrogen and oxygen was demonstrated for the first time in 1972 by Fujishima and Honda [1] in a photoelectrochemical cell PEC with an n-type semiconductor TiO$_2$ photoanode.

Since that time, many efforts have been undertaken to improve the conversion efficiency of the process but more than 30 years later this method is still far from commercialization. The reasons for this are fundamental and come as a consequence of a considerable mismatch between the spectra of light absorption in TiO$_2$ and that of solar radiation. Many other semiconductors such as GaAs had been tried as a replacement for wide-band-gap

TiO$_2$ (3.0 eV rutile, 3.2 eV anatase) before it was realized that severe requirements imposed on the photoanode material could not be met simultaneously by any existing semiconductor. These requirements include:

 (i) high stability and resistivity to corrosion and photocorrosion;
 (ii) low cost and availability;
(iii) conduction band minimum, E_C, above the H$_2$O/H$_2$ electrochemical level of water reduction $E_C > E_{H_2O/H_2}$;
(iv) valence band maximum E_V below the O$_2$/H$_2$O electrochemical level of water oxidation $E_V < E_{O_2/H_2O}$;
 (v) effective absorption of photons of the solar spectrum related to the band gap in the photon energy range of 1.6–1.9 eV.

As titanium dioxide in the form of anatase fulfils all but the last one condition, it has been admitted that the best way to the improvement of the performance of the photoelectrochemical devices would be to modify the absorption spectrum of TiO$_2$.

* Corresponding author. Tel.: +48 126172526; fax: +48 126172493.
E-mail address: radecka@agh.edu.pl (M. Radecka).

This can be achieved by shifting the fundamental absorption edge to longer wavelengths or by creating additional absorption features within the band gap. The methods tried up till now include: cation doping [2], sensitization with organic dyes [3], composite materials [4], and recently proposed, anion doping with N, C or S [5]. However, whereas it is relatively easy to affect the absorption spectra of TiO$_2$ by these methods, this is not in general true for the photocatalytic efficiency. The limiting factor is the recombination rate of the photoexcited electrons and holes.

Therefore, there are two important parameters of the electronic structure of photocatalytic semiconductors: the forbidden band gap that decides about the absorption spectrum and the flat band potential that affects the recombination probability. Fig. 1 explains the meaning of these parameters.

At the interface between the semiconducting photoanode and the electrolyte, the band bending occurs (see Fig. 1). It is a result of interface phenomena: solid-electrolyte. Moreover, the Fermi level E_F in a semiconductor and electrochemical level E_{redox} in the electrolyte are equal at the equilibrium state. The space charge region is formed at the interface. This space charge region provides a strong electric field that is indispensable for an effective separation of photoexcited electrons from holes. On the other hand, if light is absorbed in the bulk of the photoanode, the photoexcited electrons and holes are created but there is a high probability they will recombine before being used for water photolysis. Therefore, if light is absorbed in this region, charge separation and field-assisted transport are expected.

The band bending is also affected by the external voltage V_B. For a given semiconductor and electrolyte, there exists a unique potential for which the potential drop between the surface and the bulk is zero and there is no space charge layer. This is the flat band potential V_{Fb}. From the point of view of the

photoelectrochemical process it is desired to have the flat band potential large and negative.

In this work, we have used TiO$_2$ thin films as photoanodes in the process of water photolysis. Thin films were deposited by rf reactive sputtering and modified by cation dopants such as Cr and Sn.

It is well-established, especially in the case of TiO$_2$ thin films [6,7], that technological conditions of a deposition process affect the crystallographic structure, microstructure and surface properties. The substrate temperature during film growth, oxygen partial pressure and doping have a tremendous impact on the interplay between two polymorphic forms of TiO$_2$, i.e., anatase and rutile. A significant contribution from the amorphous phase dominates at lower growth temperatures [7]. It has been demonstrated [8] that the anatase is the best form of all titanium dioxide polymorphs as far as the photoactive properties are concerned.

In our previous papers [9,10] we have reported on the comprehensive structural and morphological studies of undoped and modified by cation doping TiO$_2$ thin films grown by sputtering. Here, we concentrate on the importance of the flat band potential and band gap energy (forbidden band gap) for application of these materials in the water photolysis. It should be pointed out that these parameters are very sensitive to the changes in the film microstructure and morphology.

The aim of this work is to show how different modifications of TiO$_2$ affect both the flat band potential and the forbidden band gap. The influence of these parameters of the electronic structure on the photoelectrochemical efficiency of water splitting will be demonstrated.

2. Experimental

2.1. Preparation of modified TiO$_2$ thin film photoanodes

Titanium dioxide thin films were deposited by sputtering of Ti target in Ar + O$_2$ reactive gas atmosphere onto different substrates such as Corning glass, amorphous silica, titanium and carbon foils, NaCl, etc., depending on the requirements imposed by further applications [9–14]. In the case of photoanodes, Ti foil was used as a substrate. Modification of TiO$_2$ properties was achieved by cation doping with Cr and Sn. Chromium-doped TiO$_2$ photoanodes were obtained by sputtering from mosaic Ti + Cr targets. It was possible to reach up to 16 at.% of Cr in TiO$_2$ thin films by changing the relative target area covered with Cr discs. Deposition of TiO$_2$–SnO$_2$ thin films required much higher degree of technical sophistication related to the target construction. This was a consequence of a large difference in the melting points of Ti (1940 K) and Sn (500 K) as well as in the sputtering rates of these two metals in the atmosphere containing oxygen. Photoanodes of TiO$_2$ containing up to 50 at.% of Sn were obtained by sputtering from a dielectric Ti/SnO$_2$ target of varied surface coverage with SnO$_2$.

The influence of a variety of technological parameters such as the substrate temperature T_S and oxygen partial pressure on the film properties has been investigated. Detailed description of rf and dc magnetron sputtering systems used for deposition of
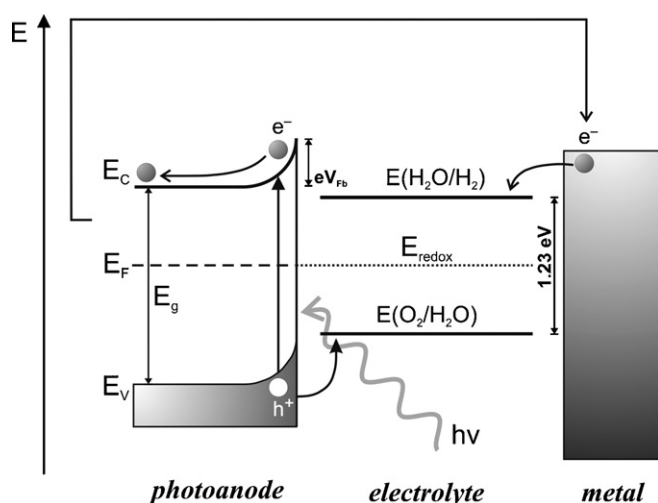

Fig. 1. Energy E diagram of the semiconducting photoanode/liquid electrolyte/metallic cathode system used for water photolysis. The flat band potential, V_{Fb} and band gap, E_g are shown. Energy levels separated by 1.23 eV and corresponding to redox reactions $E(H_2O/H_2)$, $E(O_2/H_2O)$ as well as the conduction and valence band edges are included. Upon the absorption of photon of the energy $h\nu$ a pair of electron e$^-$ and a hole h$^+$ is created.

thin films of titanium dioxide can be found in our earlier papers [9–14].

2.2. Material characterization

As-prepared thin films were subjected to a standard procedure of material characterization. The chemical composition of nonstoichiometric TiO_{2-x}, TiO_2:Cr and TiO_2–SnO_2 was determined by X-ray electron microprobe (EMP) for 1 μm-thick layers and Rutherford backscattering (RBS) for thinner films. The details are given in [9,11]. The classical methods of morphology characterization such as scanning electron microscopy (SEM) are not sensitive enough in the case of reactively deposited thin oxide films due to the smoothness of their surface. As determined from atomic force microscopy (AFM) performed at contact mode (see for example [11,13]) the surface roughness changes from 3 to 15 nm depending on the technological conditions of film deposition while the higher values are obtained for thin films annealed at 1280 K. The results of transmission electron microscopy (TEM) performed with JEM-1000 microscope indicate that thin films (up to 50 nm) of TiO_2 are amorphous to a large extent while those of SnO_2 crystallize easily even when deposited at room temperature [14]. Annealing at 770 K induces a fast crystallization of TiO_2 thin films deposited by sputtering with precipitation of large anatase grains.

Titanium dioxide thin films deposited onto amorphous silica substrates were analyzed by X-ray diffraction at GID (grazing incidence) geometry using X'Pert MPD Philips diffractometer. The anatase-to-rutile relative composition as well as the contribution from the amorphous phase were found to be a function of the substrate temperature, as shown in Fig. 2. Deposition onto unheated substrates ($T_S = 290$ K) yields a mixture of anatase and rutile with a large amount of amorphous phase. Starting from $T_S = 520$ K the anatase phase begins to dominate while at $T_S = 670$ K rutile almost completely disappears. The rutile relative contribution f_R calculated as the intensity ratio of rutile R(1 1 0) I_R and anatase A(1 0 1) I_A X-ray diffraction peaks [15]:

$$f_R = \frac{1.265 \frac{I_R}{I_A}}{1 + 1.265 \frac{I_R}{I_A}} \qquad (1)$$

decreases systematically with an increase in the substrate temperature over this range of temperatures. At temperatures higher than 770 K, the irreversible transformation from anatase to rutile initiates spontaneously [12]. The temperature and rate of this transformation depends on many factors among which the most important is the type of dopants (acceptor or donor). Acceptors such as Cr^{3+} introduce oxygen vacancies and accelerate anatase–rutile transition. As can be seen in Fig. 3, at the annealing temperature of $T_a = 970$ K the structures of undoped TiO_2 and $TiO_2 + 2.8$ at.% Cr are partially transformed into rutile while anatase is still present.

Incorporation of Sn^{4+} into TiO_2 lattice suppresses the growth of anatase crystals [11]. The rutile phase only is observed for $TiO_2 + 33$ at.% Sn as demonstrated in Fig. 3. The same conclusion can be drawn for lower amount of Sn as well as for as-sputtered and annealed films.
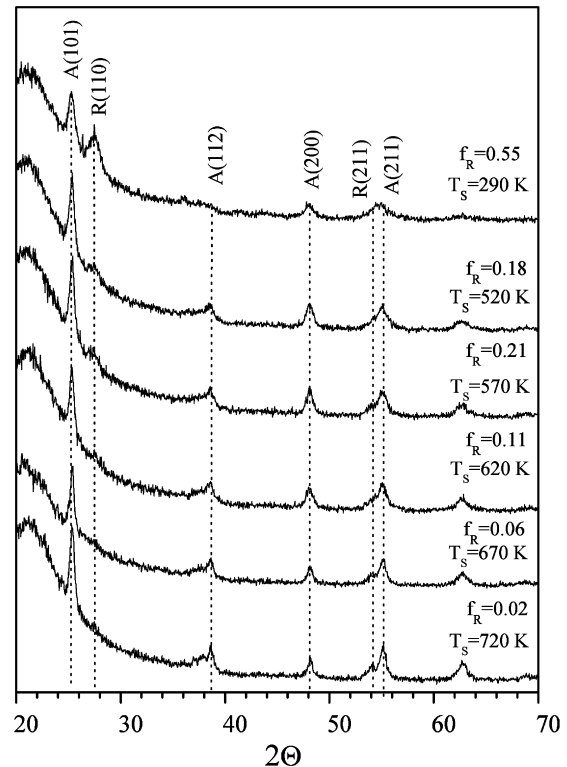

Fig. 2. The influence of substrate temperature T_S on X-ray diffraction GID patterns of undoped TiO_2 thin films deposited by rf sputtering. The film thickness is of about 200 nm. A stands for anatase; R, rutile; f_R represents the relative contribution of rutile calculated from Eq. (1).
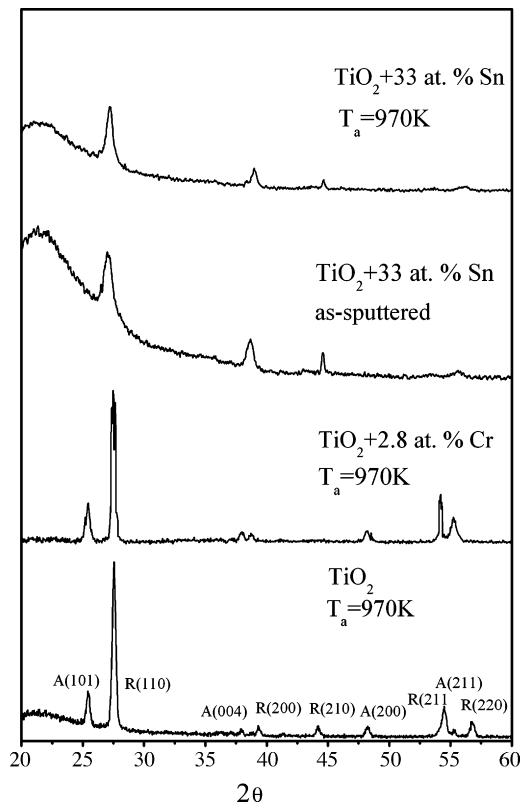

Fig. 3. X-ray diffraction GID patterns for TiO_2 thin films doped with Cr and Sn, deposited by rf sputtering and annealed at $T_a = 970$ K. The results for undoped TiO_2 annealed at 970 K are given for comparison.

2.3. Band gap energy determination

In order to determine the band gap energy E_g of transparent oxide semiconductors, the optical uv–vis spectroscopy has been performed. Optical measurements of the transmittance T and reflectance R coefficients for thin films deposited onto transparent, amorphous silica have been carried out over $\lambda = 250$–2500 nm wavelength range with Lambda 19 PerkinElmer spectrophotometer. Example of $T(\lambda)$ and $R(\lambda)$ spectra for a TiO_2 thin film of 200 nm thickness is given in Fig. 4a. The oscillations clearly seen in $T(\lambda)$ and $R(\lambda)$ result from the interference of light at both air-film and film–substrate interfaces and allow to calculate the absorption coefficient α by means of the envelope method [16]. The region over which the drastic drop of the transmittance coefficient occurs ($3.25\,eV < h\nu < 4\,eV$) corresponds to the fundamental absorption edge related to the forbidden band gap. The value of E_g can be found from the plot of $(\alpha h\nu)^m$ as a function of the photon energy $h\nu$. Fig. 4b illustrates such plot for TiO_{2-x}. The power coefficient m takes a value indicating the type of the predominant electronic transition [17] and equals 1/2 for indirect allowed transitions. This so-called Tauc plot, i.e, the following dependence:

$$\alpha h\nu = \alpha_0 (h\nu - E_g)^{1/m} \qquad (2)$$

can be fitted to the experimental data. The band gap E_g is derived from the intercept of this straight line with the photon energy
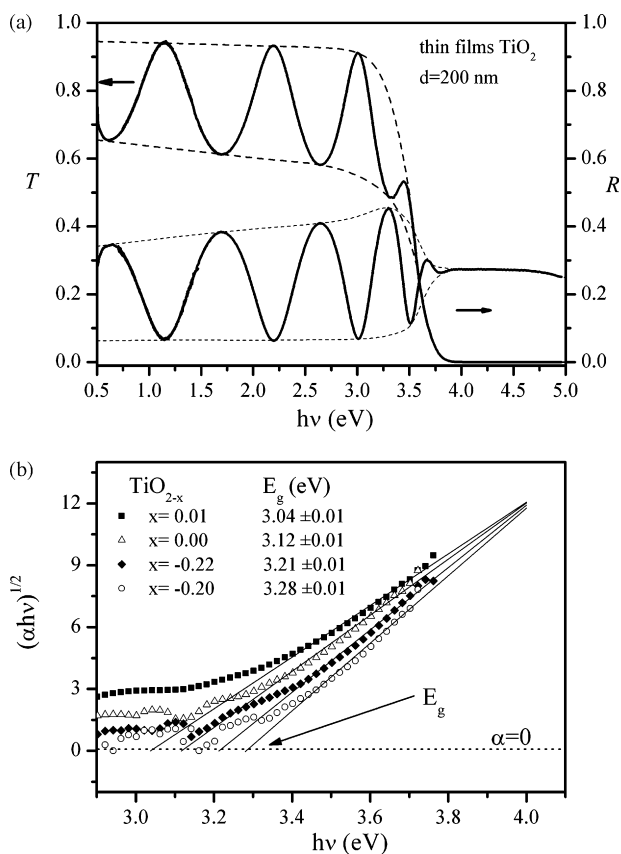
axis at $\alpha = 0$ (Fig. 4b). As one can see here, deviation x from the stoichiometric composition affects the band gap of TiO_{2-x} thin films.

2.4. Determination of the flat band potential and the photoelectrochemical experiments

There exist at least four methods of determination of the flat band potential [18]. In this work we have used two of them: the first one stems from the impedance spectroscopy in dark and the second employs the current–voltage characteristics under illumination.

The impedance spectra and capacitance of the electrode/electrolyte interface versus voltage (Mott–Schottky plots) were recorded using a frequency response analyser (Solartron Model 1260) equipped with an electrochemical interface (Solartron Model 1287).

Photoelectrochemical experiments in dark and under illumination were performed in a custom-made photoelectrochemical cell, PEC described in detail in [13]. The three-electrode PEC constructed for the experiments consists of TiO_2 photoanode, a cathode made of Pt foil covered with Pt black and SCE as a reference electrode. The electrodes are immersed in liquid electrolyte containing a buffer solution of $0.04\,M\ CH_3COOH + 0.04\,M\ H_3PO_3 + 0.004\,M\ H_3BO_3 + xKOH$ and aqueous solution of KOH. The pH of the electrolyte can be varied from 4 to 10 by changing x in the buffer solution from 10 to 14.

The PEC was illuminated with a white or monochromatic light provided by a 450 W Xe lamp and a TRIAX 180 Jobin Yvon monochromator. The power density at the photoanode was controlled by a power meter. The wavelength dependence of the incident radiation was taken into account when calculating the photoconversion efficiency and comparing the photocurrent spectra. The area of the light spot on the photoanode surface equals to $1\,mm^2$ while the average power density is of about $85\,kW\,m^{-2}$.

ANKO potentiostat was used in the measurements of current versus voltage (I–V) in order to keep a constant potential different. Keithley 6517 A electrometer recorded the photocurrent values. Kinetics of the photocurrent rise and decay, i.e., I_{Ph} versus time t, were studied in order to gain some insight into the mechanism of relaxation processes. The photocurrent spectra, i.e., $I_{Ph}(\lambda)$ were reported previously [19] while in this paper we discuss mainly the results obtained with the white light.

3. Results and discussion

3.1. Band gap energy

Band gap energy E_g, i.e., the forbidden energy is a very important parameter related to the electronic structure of a semiconducting photoanode. This parameter has to match at least the energy difference 1.23 eV between the redox levels H_2O/H_2 and O_2/H_2O required for water splitting. In the case of TiO_2 the band gap is even too high, as it amounts to 3.0 eV for rutile and 3.2 eV for anatase and in reality depends on many factors such as a degree of crystallization and doping type and level. Obviously,

Fig. 4. Determination of energy band gap E_g for TiO_2 thin films. (a) Spectral dependence of transmittance $T(\lambda)$ and reflectance $R(\lambda)$ coefficients. (b) Tauc' plot $(\alpha h\nu)^{1/2}$ vs. photon energy $h\nu$; α is the absorption coefficient.

the relative contributions from anatase, rutile and amorphous phase affect the band gap energy to a large extent in the case of thin films as shown in Fig. 5a.

Thin films of undoped TiO_2 deposited by rf sputtering are characterized by higher degree of amorphousness that the films obtained in dc magnetron sputtering [9,13] hence the energy band gap of rf sputtered TiO_2 is larger. With the increasing rutile content f_R the E_g decreases to about 3.0 eV at $f_R = 0.56$ which correlates well with the band gap of rutile. Fig. 5a illustrates dependence of E_g versus rutile/anatase ratio, on the other hand Fig. 5b demonstrates the effect of doping of TiO_2 with Cr^{+3} on the optical transitions. The solubility limit of Cr^{3+} in TiO_2 is of about 10 at.% but in the case of thin films even 16 at.% of Cr does not allow for precipitation of Cr-based phases [12].

There are two optical transitions clearly seen (Fig. 5b). The fundamental transition from the valence to the conduction band takes place at the energy E_g that obviously depends on the rutile content f_R (as shown in Fig. 5a) similarly to the case of undoped TiO_2. It has been reported previously [12] that the increased concentration of Cr^{3+} resulted in the increased rutile content in the films. Additionally, Cr^{3+} is known to create allowed states E_{dop} deep in the forbidden band of TiO_2 [20] as presented in the inset of Fig. 5b. The optical transitions between these states
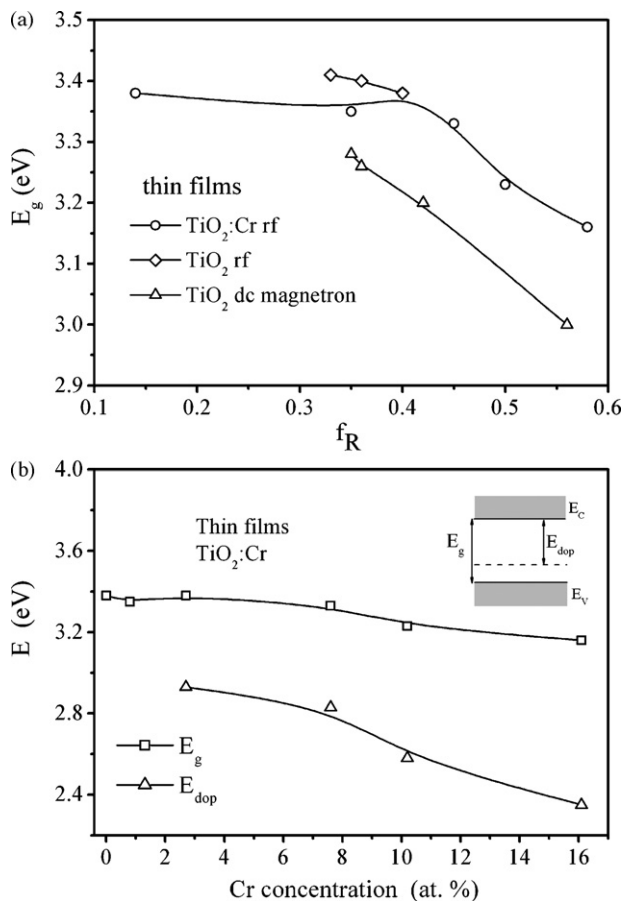
and the conduction band occur at much lower photon energies (of about 2.4–2.8 eV) than those of the fundamental absorption corresponding to the forbidden band gap E_g of TiO_2. As expected, the E_{dop} decreases considerably with the increasing concentration of Cr.

Fig. 6 shows the effect of TiO_2 doping with isovalent Sn^{4+} ions on the forbidden band gap. The ionic radius of Sn^{4+} equals to 0.071 nm and is slightly greater than that of Ti^{4+} (0.068 nm). However, the TiO_2–SnO_2 forms a solid solution over a full compositional range above a certain critical temperature that depends on the system composition [21]. The optical spectra for thin films indicate one transition only at the energy between 3.2 and 3.4 eV, which is a function of the substrate temperature and post-deposition annealing temperature. The band gap energy changes only slightly with the increasing Sn^{4+} content up to 50 at.%. It has been reported [22] that the SnO_2 additions to TiO_2 matrix affect the electronic structure of TiO_2 by creating the admixture of extended 5s Sn states to the conduction band predominantly composed of localized 3d Ti orbitals. The continuous modification of the electronic structure from d-type (TiO_2) to the s-type conduction band characteristic for SnO_2 is expected for TiO_2–SnO_2 system. The energy band gap determined from the fundamental optical transitions has been found to increase continuously with the increasing SnO_2 concentration from about 3.2–3.3. eV for TiO_2 to 3.6–3.7 eV for SnO_2 [23,24].

3.2. Flat band potential

The solid/electrolyte interface can be described by a three layer model [25]. Within the electric double layer one can distinguish: the space charge region in the electrolyte, i.e., Gouy layer (G) or diffuse part of the ionic layer 1–10 nm thick, an intermediate region called a Helmholtz layer (H) of 0.4–0.6 nm and the space charge layer in the semiconductor (SC) with thickness of 10–100 nm. These layers contribute to the total capacitance of the solid/electrolyte interface as if their capacitances where connected in series $1/C = 1/C_{SC} + 1/C_H + 1/C_G$, but as the thicknesses of both Gouy and Helmholtz layers are small as compared
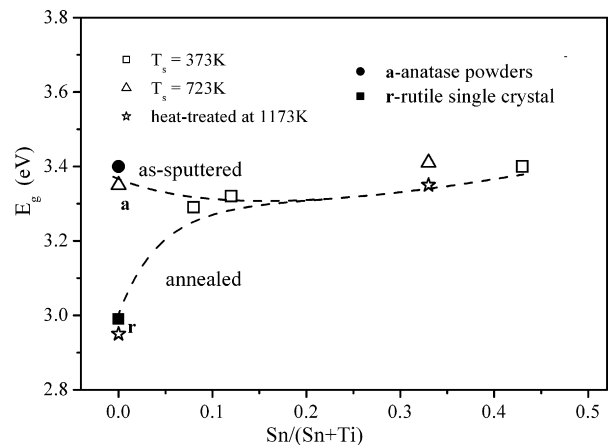

Fig. 5. (a) The energy band gap E_g as a function of the relative contribution of rutile f_R for undoped TiO_2 and Cr-doped TiO_2. (b) Energies of the optical transitions over the band gap E_g and between Cr acceptor level and the conduction band E_{dop} for TiO_2:Cr thin films deposited by rf sputtering as a function of Cr concentration.

Fig. 6. Band gap energy E_g of Sn-doped TiO_2 thin film photoanodes as a function of the atomic composition Sn/(Sn + Ti); T_s, substrate temperature. Reference data for anatase powder and rutile single crystal are given.

with that of the space charge layer in the semiconductor, their contributions to the total capacitance C can be neglected.

From the impedance spectroscopy one can find the total capacitance C of the solid/electrolyte interface and draw the so-called Mott–Schottky plot, i.e., C^{-2} as a function of the applied voltage V_B. The total capacitance C can be approximated by the capacitance C_{SC} of the depleted semiconductor electrode. This assumption is valid as long as the level of doping of the semiconductor is low.

The C_{SC} depends on the flat band potential in the following way:

$$C_{SC}^{-2} = \left(\frac{2}{\varepsilon \varepsilon_o e N_D S^2} \right) \left(V_B - V_{Fb} - \frac{kT}{e} \right) \tag{3}$$

where e is the electron charge, N_D denotes the donor density, ε is the dielectric constant of the semiconductor, ε_0 is the vacuum permittivity, T is the absolute temperature, k is the Boltzman constant and S is the surface area of the electrode.

The Mott–Schottky plots for thin films of undoped TiO$_2$ and TiO$_2$ doped with Cr are shown in Fig. 7. The results given in Fig. 7 were obtained in the measurements performed at the frequency of 10 kHz. It was verified in our earlier investigations that this frequency was within the region in which both the slope and the intercept did not depend on the frequency [26].

From the best fit to the linear part of the $C^{-2}(V_B)$ the flat band potential V_{Fb}, donor concentration N_D and the width of the depletion region W have been determined (see inset of Fig. 7).

The width W of the depletion region cannot be determined independently of the applied potential V_B as shown in the following equation:

$$W = \left(\frac{2 \varepsilon \varepsilon_0 (V_B - V_{Fb} - kT/e)}{e^2 N_D} \right)^{1/2} \tag{4}$$

where the symbols have the meaning as in Eq. (3).

The values of W plotted in the inset of Fig. 7 were obtained for $V_B - V_{Fb} = 1$ V.
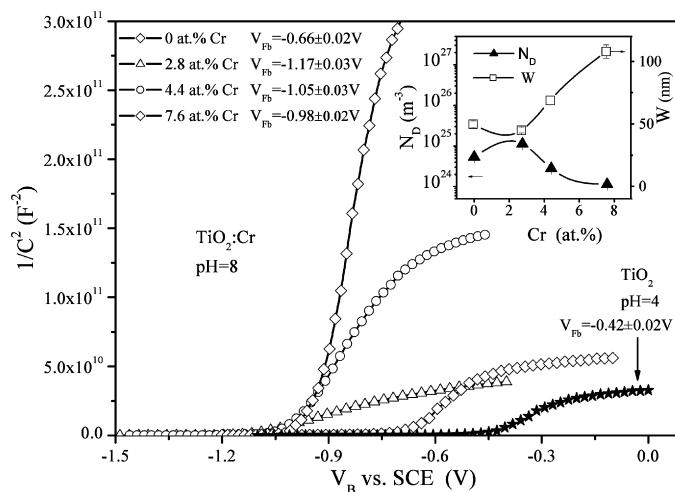

Fig. 7. Capacitance C vs. applied voltage V_B, $C^{-2}(V_B)$ Mott–Schottky plots of Cr-doped TiO$_2$ electrode at pH 4 and pH 8. V_B is determined against standard calomel electrode, SCE. Density of donors, N_D (left hand side axis) and thickness of depleted layer W (right hand side axis) vs. Cr concentration are given in the inset.
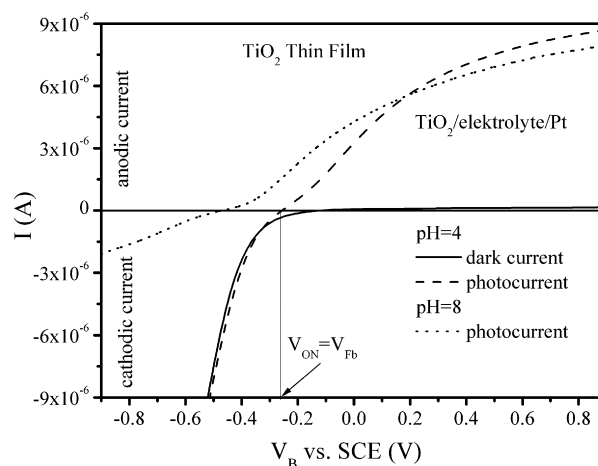

Fig. 8. Current–voltage $I(V_B)$ characteristics of a TiO$_2$ electrode in PEC in dark and under illumination with the white light at pH 4 and pH 8.

The best V_{Fb} from the point of view of the photoelectrochemical process is obtained at the doping level of 2.8 at.% of Cr in TiO$_2$. At this doping level the concentration of donors N_D is the highest.

The flat band potential has been determined from the photocurrent measurements in the PEC with TiO$_2$ photoanodes, as well. Fig. 8 shows the typical current–voltage characteristics in dark and under illumination for an undoped thin film TiO$_2$ photoanode at different pH values. The magnitude and sign of the applied external potential V_B affect the dark current and the photocurrent. The band bending decreases upon illumination of a semiconductor. The photocurrent approaches the dark current near V_{Fb}.

The threshold of photocurrent at $V_B = V_{ON}$ can be treated as a measure of the flat band potential V_{Fb}. For TiO$_2$ thin film photoanodes, the flat band potential is negative and significantly differs from zero. This means that even undoped titanium dioxide should have low enough recombination rate. As can be seen in Fig. 8, if $V_B > V_{Fb}$ the anodic photocurrent, significantly higher than the dark current, flows. Semiconductor electrode works as a photoanode in the PEC and water photolysis takes place as long as $V_B > V_{Fb}$. On the contrary, at $V_B < V_{Fb}$ much larger dark cathodic current flows and the system cannot work as a photoelectrolizer.

In order to calculate more accurately the flat band potential one has to note that in the vicinity of V_{Fb} the recombination process tends to suppress the photocurrent, hence the threshold of the photocurrent is not exactly equal to the flat band potential. Better approach to the problem of V_{Fb} determination has been proposed by Butler [27]:

$$V_B - V_{Fb} = \left(\frac{N_D}{2 e \varepsilon \varepsilon_0} \right) \left(\frac{I_{Ph}}{\alpha I_0} \right)^2 \tag{5}$$

where I_0 is intensity of the incident radiation and other symbols have the same meaning as in Eq. (3).

To apply Eq. (5), the semiconductor electrode has to be illuminated with the monochromatic light at wavelength λ comparable with λ_G corresponding to the band gap excitations. Fig. 9 presents how the flat band potential can be derived from the best
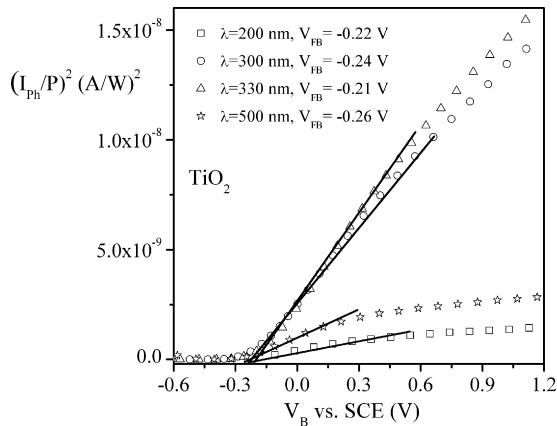
Fig. 9. Normalized photocurrent $(I_{Ph}/P)^2$ as a function of the applied voltage V_B at specific wavelengths λ in the vicinity of the fundamental absorption edge of TiO_2 photoanode; P radiation power.

linear fit of Eq. (5) to the experimental $I_{Ph}^2(V_B)$ dependence. The photocurrent was normalized to the radiation power P. Each plot has been recorded at a certain wavelength λ in the vicinity of the fundamental absorption edge. The values of the flat band potential V_{Fb} obtained this way are independent of the wavelength when λ is exactly within the region of the fundamental absorption ($\lambda = 300$–350 nm) and correspond very well with those calculated from the Mott–Schottky plots (Fig. 7).

According to Nernst equation:

$$V_{Fb} = V_{Fb}^0 - \frac{RT \ln 10}{F} pH \qquad (6)$$

where R is universal gas constant, F is Faraday constant, T is the temperature.

The flat band potential of a semiconducting photoanode is as a linear function of the pH of the electrolyte. This type of dependence along with the best fit described by Eq. (6) is given in Fig. 10. In fact, it is the parameter V_{Fb}^0, i.e., the flat band

Table 1
Comparison of the values of the flat band potential V_{FB}^0 at pH = 0 for different forms of TiO_2

Photoanode materials	V_{Fb}^0 (V)	Reference
Rutile	−0.20	[8]
Single crystal, rutile	−0.16	[28]
Single crystal, rutile	−0.27	[29]
Single crystal, rutile	−0.26	[30]
Anatase	−0.40	[8]
Anatase	−0.32	[31]
Thin films, anatase	−0.25	[32]
Thin films, anatase	−0.37	[33]
		This work
Thin films, rf, $d = 300$ nm, $f_R = 0.14$	−0.19	
$d = 500$ nm	−0.17	
Thin films dc magnetron, $d = 700$ nm, $f_R = 0.35$	−0.14	
TiO_2:Cr, rf, $d = 300$ nm		This work
2.8 at.% Cr	−0.69	
4.4 at.% Cr	−0.60	
7.6 at.% Cr	−0.55	

potential at pH = 0, that can be compared for different photoanodes. According to Kalayanansundaram and Grätzel [8] V_{FB}^0 is affected by the crystallographic structure of the TiO_2 photoanode and amounts to about −0.4 V for anatase and −0.2 V for rutile. The form of the electrode material, i.e., thin film, single crystal, polycrystalline ceramics as well as doping are also decisive factors as far as V_{FB}^0 is concerned.

Fig. 10 represents an overview of the experimental results with modified thin film photoanodes of TiO_2 obtained in the course of these studies. The straight line represents the best fit of Nernst equation (Eq. (6)) to the experimental data of V_{Fb}. The values of the V_{Fb} were calculated from the experimental data of $I_{Ph}(V_B)$ for TiO_2 photoanodes of the same thickness measured at different pH. Different series of photoanodes: of different Cr content, different thickness for rf sputtering and dc magnetron are also included. The values of V_{Fb}^0 estimated from the results
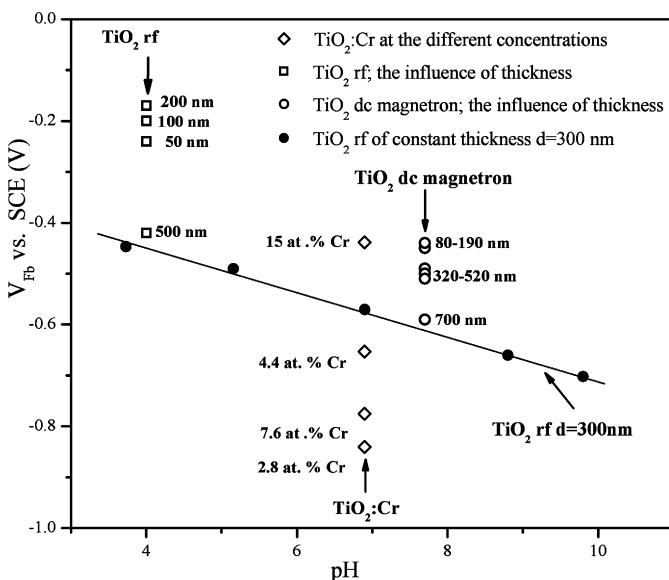

Fig. 10. The flat band potential V_{Fb} vs. pH of the electrolyte for different TiO_2 photoanodes (undoped and modified) in PEC.
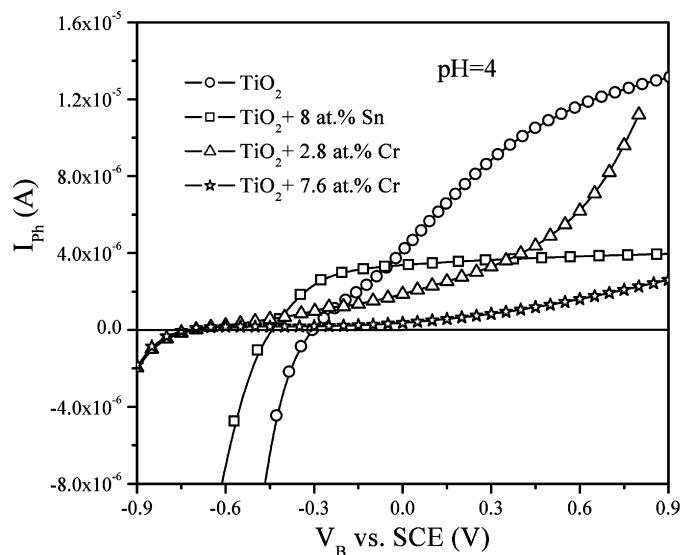

Fig. 11. Photocurrent, I_{Ph} as a function of the applied voltage V_B for TiO_2 thin film photoanodes (undoped and modified).

presented in Fig. 10 along with the values reported by other authors are listed in Table 1. It is clearly seen that the more negative values of V_{Fb}^0 are obtained for anatase. Doping with Cr increases the absolute value of V_{Fb}^0.

3.3. Photoconversion kinetics and efficiency

The effect of doping on the photocurrent I_{Ph} is clearly seen in Fig. 11. The threshold voltage depends on doping and was found to be −0.28 V versus SCE for undoped TiO_2 photoanode, −0.64 V for $TiO_2 + 2.8$ at.%Cr and −0.42 V for $TiO_2 + 8$ at.% Sn.

It is shown that the photocurrent is the highest for the film of TiO_2 and the lowest for TiO_2:Cr. This is undoubtedly a

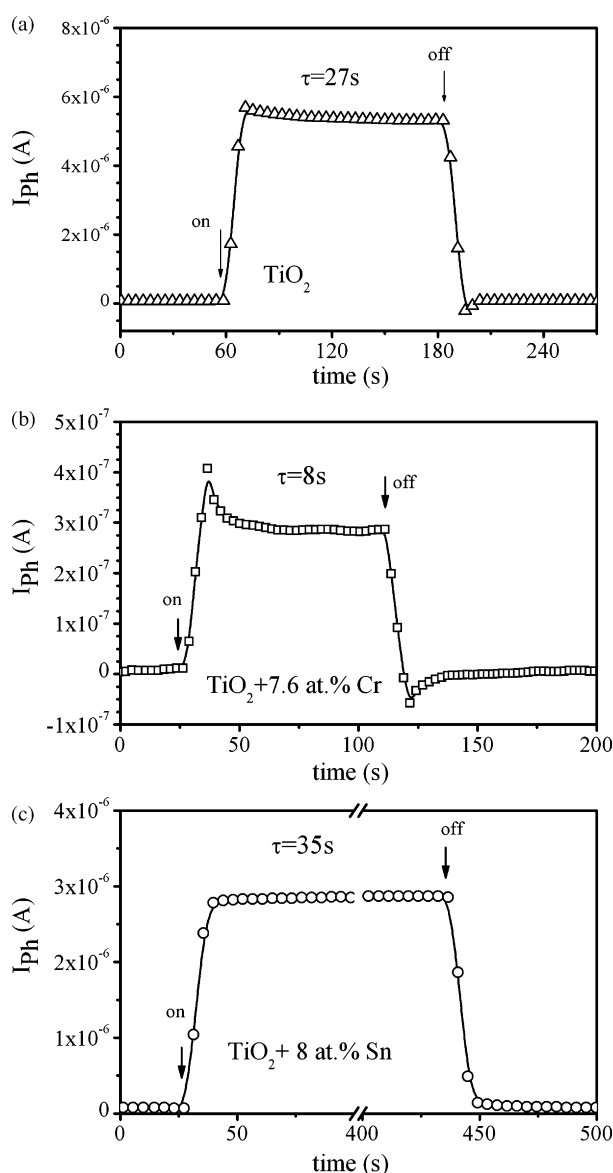consequence of lower electrical conductivity of TiO_2 doped with Cr [9].

Fig. 12 demonstrates three kinetics of the photocurrent, i.e., the responses to the sudden switching on and switching off the white light for the undoped, Cr-doped and Sn-doped TiO_2 photoanodes.

Two different types of photocurrent responses are observed. In the case of TiO_2 and TiO_2:Cr the initial increase in I_{Ph} is followed by an exponential decrease with time. This initial maximum (anodic spike) is caused by a separation of the photo-generated electron–hole pairs at the semiconductor/electrolyte interface [34]. When the light is switched off, a cathodic spike is observed due to the recombination of the conduction band electrons with the holes trapped at the surface [35].

The kinetics of I_{Ph} of the undoped sample is about three times slower than that of the Cr-doped sample as indicated by the values of the recombination time τ calculated from the exponential rise of I_{Ph} (for details see [26]). It means that Cr doping accelerates the recombination process. It is well known that incorporation of foreign ions into the TiO_2 lattice increases the concentration of point defects such as Cr'_{Ti}, $V_0^{\bullet\bullet}$, Ti_i^{4+} [36]. It seems reasonable to assume that in the case of TiO_2 the mechanism of recombination at point defects prevails.

Different shape of I_{Ph} versus time is observed for Sn-doped sample (Fig. 12c). The value of the recombination time is higher than that of undoped TiO_2. This suggests that tin does not create additional recombination centres as chromium does.

The overall efficiency of a PEC, so-called *solar conversion efficiency* η_c, has been defined by Parkinson [37] as:

$$\eta_c = \frac{\text{output power}}{\text{input power}} \qquad (7)$$

In the case of water photo-electrolysis Eq. (7) assumes a form:

$$\eta_c = \frac{\Delta G^\circ(H_2O) R(H_2) - V_B I_{Ph}}{PS} = \frac{I_{Ph}(1.23 - V_B)}{PS} \qquad (8)$$

where $\Delta G^o(H_2O)$ is a standard free enthalpy of formation of 1 mole of liquid water (kJ mol^{-1}), $R(H_2)$ is the rate of hydrogen

Fig. 12. Transient photocurrent I_{Ph} responses of (a) TiO_2, (b) TiO_2:Cr (7.6 at.% Cr) and (c) TiO_2–SnO_2 (8 at.% Sn) thin film electrodes in an electrolyte of pH 8 under illumination with white light at 0 V vs. SCE. Arrows indicate when light was turned on and off; τ is the recombination time.
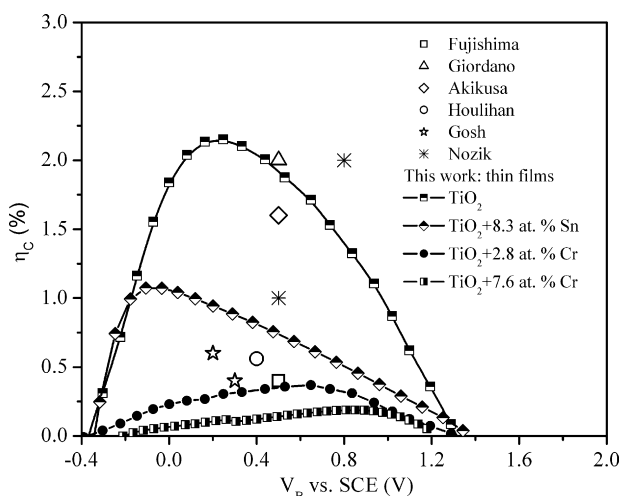

Fig. 13. Solar energy conversion efficiency η_c as a function of the applied potential V_B for TiO_2 thin film photoanodes (undoped and modified) in PEC.

Table 2
Summary of the results obtained in this work for undoped and modified thin film titanium dioxide photoanodes

Thin films photoanode	Band gap energy, E_g (eV)	Flat band potential V_{Fb} (V) at pH 4	Recombination losses τ (s)	Solar conversion efficiency η_c (%) at $V_B = 0$ V
TiO$_2$ rf, $d = 300$ nm	3.38 ± 0.05	-0.37	27	1.8
TiO$_2$ + 7.6 at.%Cr	$E_g = 3.32 \pm 0.05$	-0.72	8	0.1
	$E_{dopt} = 2.83 \pm 0.05$			
TiO$_2$ + 8 at.% Sn	3.29 ± 0.05	-0.43	35	1.0

generation (mol s^{-1}), V_B is the potential applied to the cell (V), I_{Ph} is the photocurrent within a cell, P is radiation power density (W m^{-2}) and S is the irradiated electrode area (m^2).

The parameter η_c can be calculated from the results such as those presented in Fig. 11 using Eq. (8).

Fig. 13 shows the solar conversion efficiency η_c obtained in this work for thin film photoanodes of titanium dioxide: undoped and doped with chromium and tin. These results are comparable with those of other authors [1,38–42].

Application of undoped TiO$_2$ thin film photoanodes in PEC results in the highest value of η_c. The lowest η_c, obtained when Cr-doped TiO$_2$ photoanodes are used, is related to high recombination losses.

4. Conclusions

The photolysis of water, i.e., its decomposition into hydrogen and oxygen as a result of the sunlight absorption in semiconductor electrode, is considered as the most promising source of renewable energy. The efficiency of water photolysis is determined by the intrinsic properties of the semiconducting materials applied as photoanodes. The most important parameters of the electronic structure, pertinent to the performance of the photoelectrochemical cell, PEC are: the band gap energy E_g and the flat band potential V_{Fb}. The influence of cation dopants Cr^{3+}and Sn^{4+} on E_g and V_{Fb} of TiO$_2$ thin film photoanodes was studied. The resulting PEC performance quantitatively described by recombination time τ and solar conversion efficiency η_c were derived from the dynamic changes of the photocurrent I_{Ph} and the photocurrent I_{Ph} versus voltage V_B characteristics. All these parameters are listed in Table 2.

The analysis of the results indicates that in spite of the beneficial influence of Cr^{3+} on the flat band potential, which is the most negative from all TiO$_2$ modifications, the recombination time is the shortest and the photoconversion efficiency is the lowest. This may be accounted for by the enhanced recombination of the photoelectrons and holes probably due to the fact that Cr^{3+} forms recombination centers. Acceptor level located deep in the forbidden bang gap gives additional absorption feature at longer wavelength than that corresponding to the fundamental absorption edge of TiO$_2$. However, this effect does not improve the photoconversion efficiency.

On the contrary, the influence of Sn^{4+} on the spectral dependence of the absorption in TiO$_2$ is not as promising as in the case of Cr^{3+}. The energy band gap increases in TiO$_2$–SnO$_2$ system with the increased SnO$_2$ content. Surprisingly, the flat band potential of TiO$_2$ doped with Sn is more negative than that of undoped TiO$_2$. Further comparison shows that the recombination time is slightly higher while the conversion efficiency, not as good as for undoped TiO$_2$, remains however much better than that of Cr-doped TiO$_2$.

The analysis performed in this work, indicates that an improvement of photoelectrochemical performance cannot be reached through optimization of one parameter of the electronic structure the semiconducting photoanode, only. The energy band gap that governs the absorption process and photoelectron–hole pair generation as well as the flat band potential that affects charge transfer in PEC and the recombination process are important from the point of view of the photoconversion efficiency of the PEC system but there certainly are others factors that make this picture more complicated.

References

[1] A. Fujishima, K. Honda, Nature 238 (1972) 37–38.
[2] J.M. Hermann, J. Disdier, P. Pichat, Chem. Phys. Lett. 108 (1984) 618–622.
[3] M.K. Nazeeruddin, A. Kay, I. Rodicio, R. Humphry-Baker, E. Müller, P. Liska, N. Vlachopoulos, M. Grätzel, J. Am. Chem. Soc. 115 (1993) 6382–6390.
[4] G. Zhao, H. Kozuka, T. Yoko, Thin Solid Films 277 (1996) 147–154.
[5] H. Wang, J.P. Lewis, J. Phys. Condens. Mat. 18 (2006) 421–433.
[6] W.T. Pawlewicz, P.M. Martin, D.D. Hays, I.B. Mann, Proc. SPIE 325 (1982) 105–116.
[7] P. Löbl, M. Huppertz, D. Mergel, Thin Solid Films 251 (1994) 72–79.
[8] K. Kalayanansundaram, M. Grätzel, Coordin. Chem. Rev. 77 (1998) 347–414.
[9] K. Zakrzewska, M. Radecka, M. Rekas, Thin Solid Films 310 (1997) 161–166.
[10] K. Zakrzewska, Thin Solid Films 391 (2001) 229–241.
[11] K. Zakrzewska, M. Radecka, J. Przewoźnik, K. Kowalski, P. Czuba, Thin Solid Films 490 (2005) 101–107.
[12] M. Radecka, K. Zakrzewska, M. Wierzbicka, A. Gorzkowska, S. Komornicki, Solid State Ionics 157 (2003) 379–386.
[13] A. Brudnik, A. Gorzkowska-Sobaś, E. Pamuła, M. Radecka, K. Zakrzewska, J. Power Sources 173 (2007) 774–780.
[14] F. Edelman, H. Hahn, S. Seifried, C. Alof, H. Hoche, A. Balogh, P. Werner, K. Zakrzewska, M. Radecka, P. Pasierb, A. Chack, V. Mikhelashvili, G. Eisenstein, Mater. Sci. Eng. B69–70 (2000) 386–391.
[15] R.A. Spurr, H. Myers, Anal. Chem. 29 (1957) 760.
[16] J. Szczyrbowski, J. Phys. D: Appl. Phys. 11 (1978) 583–591.
[17] J. Tauc, Mater. Res. Bull. 5 (1970) 721–730.
[18] M. Radecka, M. Rękas, K. Zakrzewska, Trends Inorg. Chem. (2007), in print.

[19] A. Gorzkowska-Sobaś, E. Kusior, M. Radecka, K. Zakrzewska, Surf. Sci. 600 (2006) 3964–3970.

[20] G. Campet, J. Verniolle, J.-P. Doumerc, J. Claverie, Mater. Res. Bull. 15 (1980) 1135–1139.

[21] V.S. Stubican, A.H. Schultz, J. Am. Ceram. Soc. 55 (1968) 290–291.

[22] M. Radecka, P. Pasierb, K. Zakrzewska, M. Rekas, Solid State Ionics 119 (1999) 43–48.

[23] K.M. Glassford, J.R. Chelikowsky, Phys. Rev. B 46 (1992) 1284–1289.

[24] J. Melsheimer, D. Ziegler, Thin Solid Films 129 (1985) 35–41.

[25] H. Gerischer, in: B.O. Seraphin (Ed.), Solar Energy Conversion, Solid State Physics, Springer-Verlag, New York, 1979.

[26] M. Radecka, M. Wierzbicka, S. Komornicki, M. Rekas, Phys. B 348 (2004) 160–168.

[27] M.A. Butler, J. Appl. Phys. 48 (1977) 1914–1920.

[28] E.C. Dutoit, F. Cardon, W.P. Gomes, J. Appl. Electrochem. 8 (1978) 247–252.

[29] L.J. Handley, A.J. Bard, J. Electrochem. Soc. 127 (1980) 338–343.

[30] M.S. Wrighton, P.T. Wolczanski, A.B. Ellis, J. Solid State Chem. 22 (1977) 17–29.

[31] D. Duonghong, J. Ramsden, M. Grätzel, J. Am. Chem. Soc. 104 (1982) 2977–2985.

[32] L. Kavan, M. Grätzel, Electrochim. Acta 40 (1995) 643–652.

[33] C. da Fonseca, S. Boudin, M.C. Belo, J. Electroanal. Chem. 379 (1994) 173–180.

[34] A. Hagfeldt, H. Lindström, S. Södergren, S.-E. Lindquist, J. Electroanalyt. Chem. 381 (1995) 39–46.

[35] N.W. Duffy, L.M. Peter, R.M.G. Rajapakse, K.G.U. Wijayantha, Electrochem. Commun. 2 (2000) 658–662.

[36] J. Nowotny, M. Radecka, M. Rekas, J. Phys. Chem. Solids 58 (1997) 927–937.

[37] B. Parkinson, Acc. Chem. Res. 17 (1984) 431–437.

[38] J.F. Houlihan, D.B. Armitage, T. Hoovler, D. Bonaquist, D.P. Madacsi, L.N. Mulay, Mater. Res. Bull. 13 (1978) 1205–1212.

[39] A.J. Nozik, Nature 271 (1978) 137.

[40] A.K. Ghosh, H.P. Maruska, J. Electrochem. Soc. 124 (1977) 1516–1522.

[41] J. Akikusa, S.U.M. Khan, Int. J. Hydrogen Energy. 22 (1997) 875–882.

[42] N. Giordano, V. Antonucci, S. Cavallaro, R. Lembo, J.C.J. Bart, Int. J. Hydrogen Energy 7 (1982) 867–872.